JOURNAL OF AGRICULTURAL AND FOOD CHEMISTRY

J. Agric. Food Chem. **2006,** *54,* 6733−6740 **6733**

Salt-Induced Changes in Pork Myofibrillar Tissue Investigated by FT-IR Microspectroscopy and Light Microscopy

ULRIKE BÖCKER,*,†,‡ RAGNI OFSTAD,† HANNE CHRISTINE BERTRAM,§ BJØRG EGELANDSDAL,‡ AND ACHIM KOHLER†

Centre for Biospectroscopy and Data Modelling, Matforsk AS, Norwegian Food Research Institute, Osloveien 1, N-1430 Ås, Norway, Department of Chemistry, Biotechnology and Food Science, Norwegian University of Life Sciences, P.O. Box 5003, N-1432 Ås, Norway, and Department of Food Science, Danish Institute of Agricultural Sciences, Research Centre Foulum, P.O. Box 50, DK-8830 Tjele, Denmark

FT-IR microspectroscopy and light microscopy were used to investigate pork muscle *musculus semitendinosus* samples, taken from three animals, that were subjected to brine salting at different concentrations (0.9, 3, 6, and 9% NaCl). Differences in spectral characteristics and in microstructure were observed in meat from animals differing in initial pH and varying salt concentrations. The FT-IR data displayed changes in the amide I region from 1700 to 1600 cm^{-1}. This spectral range was analyzed by principal component analysis (PCA) and partial least-squares regression (PLSR). These methods revealed correlations between the spectral data and the different animals, salt content, moisture content, pH value, and myofiber diameter. A shrinking share of α-helical components was related to an increase in salt concentration in the muscle. At the same time, a greater share in nonhydrogenated C═O groups (1668 cm^{-1}) was related to an increase in salt concentration in the meat. The share of aggregated β-strands differed with respect to the different animals but was not influenced by salt concentration. The meat at higher pHs (>6) had less aggregated β-strands than that at lower pHs (5.6−5.7). It could be demonstrated that simultaneous with changes in microstructure, pH value, salt, and moisture content were alterations in the protein amide I region as measured by FT-IR microspectroscopy, revealing a relationship between these biophysical and chemical parameters and secondary protein structure attributes.

KEYWORDS: FT-IR microspectroscopy; light microscopy; pig muscle; salting; curing

INTRODUCTION

Curing meat has a long tradition, and cured meat products have a substantial market share of the total processed red meat sale. The industry is aiming at reducing the salting time and increasing the yield while ensuring microbiological safety with preferably no detrimental effects on sensory qualities like flavor, texture, and juiciness. At the same time, there is an increasing consumer demand for high-quality cured products, and thus, there is a need for improved knowledge about which manufacturing factors influence quality. Recent studies have shown that raw meat quality, composition, and pH as well as the salt content and temperature of the brine influenced the moisture diffusivity and texture of the dry-cured ham (*1*−*4*). During salting, NaCl causes swelling of the muscle and an increase in the water-holding capacity (*5*). Maximum swelling is reached for concentrations between 0.85 (∼5%) and 1 M (∼6%), whereas higher concentrations again reduce the swelling effect (*6*−*8*). The water-holding capacity is highly influenced by structural changes, i.e., myofibril swelling or contraction, which is affected by both ionic strength and pH (*7*−*9*). Salt-induced swelling and water expulsion will also depend on the post-mortem status of the meat as well as the type of muscle and fibers studied (*10*−*14*).

Proteins and especially the myofibrillar proteins are the most important functional components of muscle, with myosin (∼54%), actin (∼20%), and titin (∼10%) being the most abundant in the myofibrillar protein fraction. α-Helical coiled coil structure makes up the rod part of myosin, while the head region consists of α-helix structure (ca. 48% of the amino acid residues in this conformation) accompanied by β-strands connected by turns and loops (*15*). One-quarter of G-actin secondary structure is made up of α-helical structure, while one-quarter is β-pleated sheet and the rest random coil structure; F-actin comes about in the form of a left-handed helix (*15*, *16*). In several studies using UV Raman spectroscopy, FT-IR spectros-

* To whom correspondence should be addressed: Matforsk AS, Norwegian Food Research Institute, Osloveien 1, N-1430 Ås, Norway. Phone: +47 64 97 01 00. Fax: +47 64 97 03 33. E-mail: ulrike.bocker@matforsk.no.
† Norwegian Food Research Institute.
‡ Norwegian University of Life Sciences.
§ Danish Institute of Agricultural Sciences.

10.1021/jf060178q CCC: $33.50
Published on Web 08/12/2006

copy, circular dichroism, and NMR spectroscopy, it was determined that titin (also known as connectin) consists mainly of β-structures (*17*−*21*).

Chemical and physical changes that affect the structure of the muscle occur mainly through desolubilization and/or aggregation of the proteins and dehydration of the muscle. Differential scanning calorimetry (DSC) studies showed clear effects of ionic strength on the thermal denaturation of myosin and muscle proteins (*22*−*24*). These changes in the structure of the myofibrillar proteins were related to alterations in the tertiary structure of myofibril proteins. However, techniques like circular dichroism, which is dependent on the work being done at low concentrations only, and DSC do not allow insight into alterations in protein structures and into the spatial distribution of the proteins which may be related to salt uptake and water uptake and/or loss.

At present, the relationship between salt-induced myofiber swelling or shrinkage and changes in the highly organized protein structures is still a rather unexplored area. Therefore, FT-IR spectroscopy and histology were combined in this study to facilitate a simultaneous characterization of protein structures and muscle microstructure during salting of pork.

The FT-IR microscope provides a versatile instrument for rapid biological microanalysis, which can be used to detect slight alterations in the chemical composition within intact cells and tissues (*25*, *26*). Since FT-IR spectroscopy is based on information from fundamental molecular vibrations, it allows the investigation of the structure of peptides and proteins (*27*, *28*), e.g., during salting of meat. The amide I band in the frequency region from 1700 to 1600 cm^{-1} is the most prominent feature in the FT-IR spectrum of the muscle myofibers. It is by far the best-characterized band with respect to conformational studies of proteins and commonly used in secondary structure analysis (*27*, *28*). The amide I band is mainly due to the carbonyl stretching vibration with a minor contribution of C−N stretching and N−H bending vibrations, and it mostly depends on the secondary structure of the protein backbone.

A major advantage of FT-IR microspectroscopy is that it can easily be combined with histological investigations, as it requires a similar sample preparation, and thus, specific features can be studied on parallel histologic sections both histochemically and spectroscopically. Kirschner et al. (*29*) used FT-IR microspectroscopy and FT-IR imaging to monitor heat-induced denaturation in beef. The study revealed conformational changes in the amide I region, i.e., a decrease in α-helical structure content and an increase in aggregated β-sheet content at higher temperatures. Most recently, by applying both low-field NMR relaxometry and FT-IR microspectroscopy in a study of cooked meat, the chemical−physical properties of the water within the meat could be associated with structural changes in muscle proteins that occur during heating (*30*).

The aim of this work was to study the effect of brine salting on muscle protein structure by FT-IR microspectroscopy. The effect of salting was investigated with regard to initial muscle pH and fiber type. The experiment was performed with samples consisting of mainly red or white fibers and with meat with different initial pHs. In parallel with the microspectroscopic analysis, changes in the microstructure of the samples were evaluated by light microscopy. Analysis of variance by partial least-squares regression (ANOVA-PLSR) was used to relate the changes observed in myofiber swelling or shrinkage and moisture to alterations in the amide I region of the FT-IR spectra at different salt concentrations.

MATERIALS AND METHODS

Animal Treatment and Sample Preparation. To obtain meat with differences in the initial pH, the meat was collected from animals with varying preslaughter histories (offspring of Duroc/Landrace boars crossbred with Landrace/Yorkshire sows). One animal ("animal 1") did not experience any specific preslaughter treatment. Animal 2 was exercised on a treadmill at a speed of 3.8 km/h for approximately 20 min and was electrically stunned prior to being slaughtered (*31*). Animal 3 was injected with adrenaline (subcutaneous injection, 0.2 mg/kg of live weight) 16 h before being slaughtered using the method described in ref *32*. Animal 1 and animal 3 were stunned with 80% CO_2 for 3 min before being slaughtered. All three pigs were exsanguinated and scalded at 62 °C for 3 min and cleaned and eviscerated within 30 min postmortem. The carcasses were split and kept at 12 °C and then transferred to a chill room (4 °C) 3 h post-mortem. The pH value was determined in *musculus semitendinosus* 24 h post-mortem according to the procedure described in ref *33*. Twenty-four hours post-mortem, *musculus semitendinosus* was excised and divided into two parts: one known to consist predominantly of red muscle fibers (red muscle) and one known to consist mostly of white fibers (white muscle). The pH_{24} values in the red and white parts of *musculus semitendinosus* were 5.57 and 5.56, 5.71 and 5.59, and 6.67 and 6.29 for animals 1−3, respectively. From each part, 4 cm × 4 cm × 4 cm samples were excised and placed into 0.9, 3, 6, and 9% NaCl solutions with 10 mM sodium acetate buffer (pH 5.5), and 0.05% NaN_3 was added. To avoid substantial dilution of the brine during salting, the mass ratio of brine to meat was 10:1. The samples were kept in the brine for 8 days at 4 °C and were stored on shaking tables.

Muscle blocks of approximately 7 mm × 7 mm × 2 mm were excised from each sample, embedded in O.C.T. compound (Tissue-Trek, Electron Microscopy Sciences, Hatfield, PA) and snap-frozen in liquid N_2. All blocks were stored at −80 °C until they were cryo-sectioned. The sectioning was performed in a cryostat (model CM 3050 S, Leica, Nussloch, Germany) transversely to the fiber direction. Sections (8 μm thick) were prepared and thaw-mounted on infrared transparent CaF_2 slides (2 mm thick) for the FT-IR microscopic measurements. Parallel sections were collected for light microscopy. The slides for FT-IR microspectroscopic measurements were stored in a desiccator. FT-IR spectra were collected 1 day after cryo-sectioning.

Light Microscopy and Image Analysis. For light microscopic observation, the cryo-sections were stained with alum hematoxylin (*34*) (Sigma-Aldrich Norway AS, Oslo, Norway) for 10 min, washed in tap water, counterstained with hexamine (VWR International AS, Oslo, Norway) for 3 min, rinsed again, and stained in erythrosine (VWR International AS) for a further 3 min. Subsequently, the slides were rinsed, dehydrated in ethanol (increasing concentration) and xylene, and finally mounted with a Eukitt mounting medium (VWR International AS).

The sections were examined with a Leica DMLB microscope, and images were acquired with an RT color camera (SPOT Diagnostic Instruments, Inc.) at 100× magnification. Two hundred fibers per image were used to determine the fiber diameter using Image-Pro Plus 4.5 (MEDIA CYBERNETICS, The Imaging Experts, Silver Springs, MD). Microscopic examinations were carried out in replicate for two blocks of each sample condition (animal, red and white muscle part, and salt concentration).

The images taken as light micrographs correspond to the same areas from which spectra were collected by FT-IR microspectroscopy on parallel cryo-sections.

Chemical Analysis. The pH value of the salted samples was determined by using a Beckman pH-meter (Beckman Instruments Inc.) equipped with a Mettler-Toledo InLab 427 electrode (Mettler-Toledo GmbH, Urdorf, Switzerland).

NaCl content in the salted muscle samples was determined as water-soluble Cl^- and was determined by titration with a Corning salt analysator 926 (chloride analyser 926 Corning, Corning Medical and Scientific, Halstead, England) (*35*). The cured samples were also analyzed for their moisture content (%) by being dried at 103 °C according to the procedure of the "Nordisk Metodikkommite for næringsmidler, NMKL-metode nr 23" from 1991 (*36*) and is given as

the average of two parallel runs. Due to lack of sample material, pH and NaCl content data were acquired by two readouts from one sample only.

FT-IR Microspectroscopy. The analysis of the tissue sections was performed on an IR microscope (IRscope II) connected to an Equinox 55 FT-IR spectrometer (both from Bruker Optics). The Bruker system was controlled with an IBM-compatible personal computer running OPUS-NT, version 4.0. The microscope was equipped with a computer-controlled x,y stage. IR spectra were collected from single myofibers (30−60 μm in diameter depending on the salt treatment and pH) in transmission mode from 4000 to 1000 cm^{-1} with a spectral resolution of 6 cm^{-1} using a mercury−cadmium−telluride (MCT or HgCdTe) detector. For each spectrum, 256 interferograms were co-added and averaged. The microscope, which was sealed using a specially designed box, and the spectrometer were purged with dry air to reduce spectral contributions from water vapor and CO_2. A background spectrum of the CaF_2 substrate was recorded before each spectrum was measured to account for variations in water vapor and CO_2.

For every sample (animal, red and white muscle part, and salt concentration), two different blocks, taking one section each, were analyzed by light microscopy and FT-IR microspectroscopy. In total, 12 spectra of single myofibers from two different locations (six spectra from each location) were analyzed per cryo-section. The two blocks for every sample were analyzed with a time difference of 2 months and in the following are termed block A (first measurements) and block B (measurements 2 months later). A total of 720 spectra were used: 6 spectra from each area × 2 areas per section × 2 muscle parts × 5 salt concentrations × 2 blocks per concentration × 3 animals.

The samples taken out 24 h post-mortem were not included in the multivariate analyses of the FT-IR spectra (576 spectra in total). This is due to the fact that the salted samples were subjected to conditions (stored at 4 °C for an additional 8 days before being frozen in liquid N_2 and being stored frozen at −80 °C) different from those for the samples taken 24 h post-mortem, which may introduce additional differences into their spectral signature. Instead, the samples salted at 0.9% NaCl served as reference to physiological conditions.

Preprocessing of the FT-IR Spectra and Data Analysis. The infrared spectra were preprocessed using extended multiplicative signal correction (EMSC) (*37*, *38*). EMSC allows the separation of physical light scattering effects (as baseline, multiplicative, linear, and quadratic wavenumber-dependent effects) from chemical information in spectra. After the spectra had been preprocessed by EMSC, the second derivative of the spectra was calculated by applying a nine-point Savitzky−Golay filter (*39*). For all data analysis in this paper, the amide I region (1700−1600 cm^{-1}) was used, since the amide I region contains the most detailed information about the secondary structure of proteins (*28*).

The data were analyzed by principal component analysis (PCA) and partial least-squares regression (PLSR) (*40*). In this paper, PCA was used for the investigation of the main variations in the amide I region of the FT-IR spectra. For presentation purposes, the figures in this paper are based on averaged spectra (average of 12 spectra per condition). Multivariate analysis carried out with all single spectra (576 in total) gave similar results, which are not shown.

To investigate the effect of the design on sample characteristics such as chemical data or FT-IR spectra, partial least-squares regression (PLSR), i.e., ANOVA-PLSR, was used (*41*). In ANOVA-PLSR, the design variables are used as the **X**-matrix and the measured variables (FT-IR data) are used as the **Y**-matrix (*40*). The **X**-matrix for the design is defined by using indicator variables 0 and 1 for the design factors. Every condition, e.g., animal 1 salted at 6%, was defined as one variable. Zero or 1 indicated if one condition applied for a sample. Second derivatives were calculated to enhance the resolution of the amide I band. For presentation purposes, the second-derivative bands used in ANOVA-PLSR were multiplied by −1. The results of the ANOVA-PLSR were then studied using so-called correlation loading plots. The correlation loading plot shows the correlation of the *X* and *Y* variables to the PLSR components and can therefore be used to study how the design factors are correlated with the measured variables within the model.

All preprocessing and data analysis was performed using The Unscrambler (version 9.2, CAMO Process AS).

Table 1. Results from the Chemical Analysis and the Average Myofiber Diameter of the Cured Samples

		% NaCl				
	muscle	in brine	in meat	pH	% moisture	diameter (μm)
animal 1	red	0.9	1.03	5.64	80.37 ± 0.88	63.65 ± 14.34
		3	2.93	5.60	81.32 ± 0.32	65.24 ± 14.34
		6	5.45	5.60	80.34 ± 0.09	64.26 ± 19.53
		9	8.08	5.57	77.77 ± 0.11	56.86 ± 17.58
	white	0.9	1.08	5.66	78.75 ± 0.20	68.86 ± 17.14
		3	2.80	5.58	79.74 ± 0.23	68.20 ± 17.89
		6	5.44	5.59	77.33 ± 0.31	68.62 ± 17.57
		9	8.30	5.56	77.37 ± 0.05	60.47 ± 15.32
animal 2	red	0.9	1.07	5.68	78.82 ± 0.28	53.96 ± 14.82
		3	2.87	5.64	79.43 ± 0.08	60.53 ± 15.05
		6	5.51	5.62	78.1 ± 0.12	52.29 ± 13.31
		9	8.21	5.56	77.32 ± 0.12	56.75 ± 15.00
	white	0.9	1.04	5.60	77.00 ± 0.02	58.52 ± 13.86
		3	2.60	5.59	79.35 ± 0.25	60.32 ± 15.08
		6	5.72	5.57	78.46 ± 0.21	65.65 ± 17.40
		9	8.75	5.50	76.26 ± 0.04	58.73 ± 13.78
animal 3	red	0.9	1.01	6.39	82.92 ± 0.07	56.04 ± 14.33
		3	2.79	6.36	83.83 ± 0.42	66.69 ± 19.90
		6	5.75	6.15	81.46 ± 0.44	63.59 ± 19.80
		9	8.01	6.10	80.10 ± 0.23	61.37 ± 17.99
	white	0.9	1.19	6.04	80.69 ± 0.11	63.67 ± 16.44
		3	2.63	6.04	82.16 ± 0.28	73.63 ± 21.03
		6	5.04	6.07	78.95 ± 0.50	72.11 ± 19.10
		9	8.14	5.75	78.52 ± 0.39	60.47 ± 17,72

RESULTS

Chemical Characteristics and Microstructure. Table 1 summarizes the sample characteristics after salting. As expected, the NaCl content of the meat increased as the salt content in the brine increased. All meat samples revealed a salt content lower than that of the corresponding brine. Animal 3 had a higher pH than animals 1 and 2. In general, the pH value of all samples decreased with an increase in salt concentration. The moisture content increased with an increase in salt content, reaching its maximum when salted at 3% NaCl (for corresponding NaCl percents in the meat, see **Table 1**). At all salt concentrations, samples from animal 3, with the highest pH, contained more moisture than the samples from animals 1 and 2. Moreover, with increasing salt concentrations, the myofiber diameter as measured on the light micrographs reached a maximum when the samples were salted in the 3% brine for animal 3 and in the 6% brine for animals 1 and 2. The smallest diameter was observed in the samples cured in 0.9 and 9% brine for all three animals. For all three animals, the myofiber diameter was generally smaller for samples from the red muscle part of the muscle than for samples from the white muscle part.

To illustrate the individual differences of the animals and the effects of the curing conditions, selected images of transverse cryo-sections of samples from the red muscle part are shown in **Figure 1**. The images were carefully selected from many and represent typical attributes. Similar features were observed for the samples from the white muscle part (not shown).

For the unsalted samples, both samples from animal 1 and animal 3 exhibited an intact and dense structure with the myofibers appearing well attached. In contrast to that, the myofibers of animal 2 appeared to be detached with extended extracellular space.

After the samples had been salted, the myofibers became more detached and the extracellular space grew wider in animals 1 and 2. At the highest salt concentration, the fibers of these two animals (1 and 2) appeared to be shrunken and their shape was uneven and edged. In the samples from animal 3, the myofibers

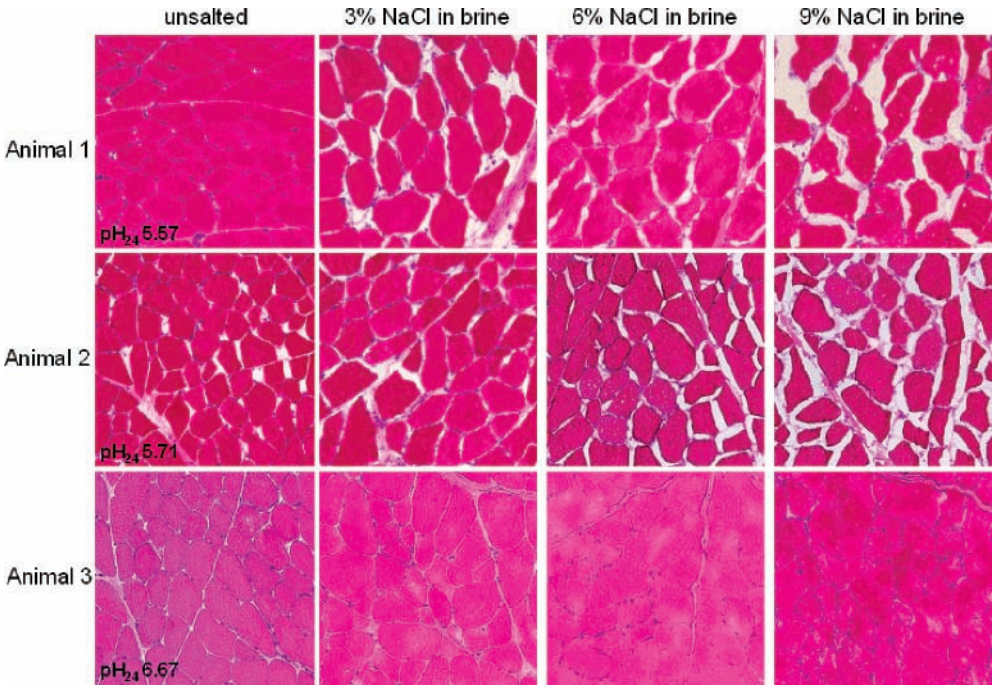

Figure 1. Selected light microscopic images (hematoxylin erythrosine staining) from the red muscle part of all three animals (myofibers stained red, nuclei stained blue). The salt concentrations of the samples are given (as percent NaCl in the brine).

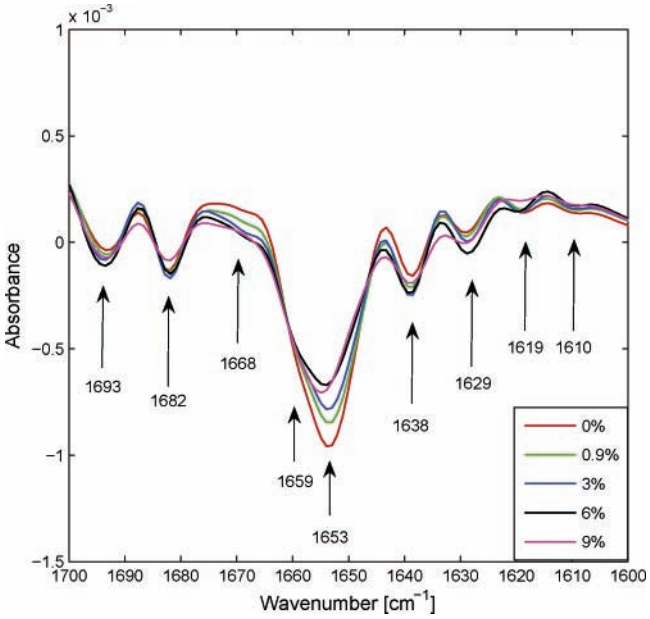

Figure 2. Amide I region second-derivative spectra derived from EMSC pr-processed spectra of control samples with different salt concentrations all from the red muscle part. The salt concentration given as percent NaCl in the brine is indicated by different colors explained in the legend.

were well attached for all salt concentrations, but the myofibers turned more amorphous with the dense appearance of the structure with an increase in salt content. The higher the salt concentration, the harder it was to distinguish between individual myofibers.

FT-IR Microspectroscopy. Figure 2 shows the average spectra (average of 24 spectra, from two blocks per salt concentration with 12 spectra per block) of four different salt concentrations and the 0 sample for the red muscle of the control animal. The spectra are presented as the second derivative in the amide I region (1700−1600 cm^{-1}). The positive bands in the unprocessed spectra correspond to the negative bands in the second-derivative spectra. By visual inspection, bands were identified at the following wavenumbers: 1610, 1619, 1629, 1638, 1653, 1659, 1668, 1682, and 1693 cm^{-1}. Similar amide I band features were observed for the white muscle. We observed bands at similar positions in an earlier study (*30*), as we investigated heat-treated pork muscle tissue by FT-IR microspectroscopy.

The band at 1653 cm^{-1} can be assigned to C═O stretching vibrations in α-helical structures in the myofibrillar proteins (*27*). This band decreased in magnitude with an increase in salt concentration (**Figure 2**), implying a loss of α-helical components. Wavenumbers associated with β-structures may originate either from aggregated β-strands or native β-sheet conformations, the first occurring intermolecularly and the latter intramolecularly. Due to transition dipole coupling in β-conformational structures, the C═O band for antiparallel β-components is split and gives rise to one band above and one below the α-helical band at 1653 cm^{-1}. Depending on the distance of the C═O components in the chains, that is, the strength of the influence on neighboring chains, the distance can be as large as approximately 60 cm^{-1} (*28*). Jackson and Mantsch (*42*) assign bands occurring from 1610 to 1628 cm^{-1} to denatured aggregated β-sheet components (intermolecular), while they relate a band between 1630 and 1640 cm^{-1} to antiparallel β-sheet structures (intramolecular). Considering the phenomenon of the band splitting due to transition dipole coupling, bands found at 1682 and 1693 cm^{-1} may be the weaker components of the antiparallel β-sheet structures and the denatured aggregated β-sheet components, respectively. The corresponding lower-wavenumber bands are possibly related to denatured aggregated β-sheet structures that are found at 1619 and 1628 cm^{-1}, while the band at 1638 cm^{-1} may be related to antiparallel β-sheets. At 1640 cm^{-1}, a strong non-protein contribution from O−H bending of water also has to be expected, which is overlapping with the possible low-frequency contribution of antiparallel β-sheets (*43*).

The features at 1659 and 1668 cm^{-1} appear to be not very prominent, but bands at almost similar positions (1660 and 1668

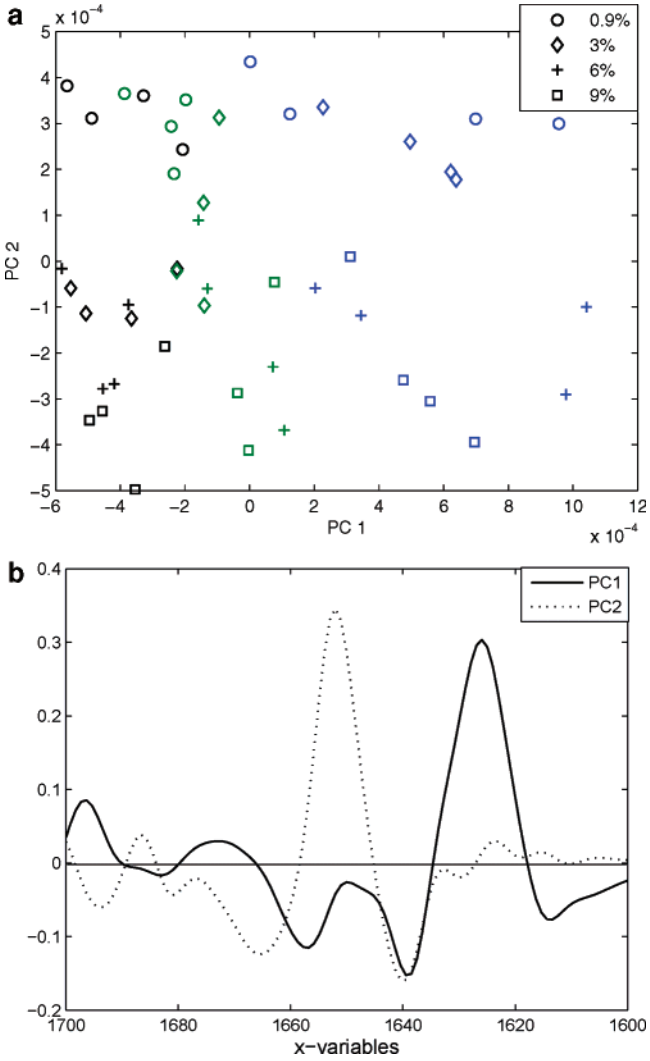

Figure 3. (**a**) PCA score plot of the variation between second-derivative spectra in the range between 1700 and 1600 cm^{-1}. The explained variances for PC 1 and PC 2 are 64 and 23%, respectively. Marked in green are data for animal 1, in blue data for animal 2, and in black data for animal 3. The salt concentration given as percent NaCl in the brine is indicated by symbols explained in legend. (**b**) PCA loadings of PC 1 and PC 2 of second-derivative spectra between 1700 and 1600 cm^{-1}. The explained variances for PC 1 and PC 2 are 64 and 23%, respectively.

cm^{-1}) were found in spectra of heat-treated pork (*30*) and are therefore considered relevant. The region between 1660 and 1670 cm^{-1} is commonly assigned to random structure (*44*). Jackson and Mantsch (*42*) consider spectral features between 1666 and 1670 cm^{-1} to be related to nonhydrogenated C═O groups which are sterically constrained and may be involved in only weak dipole−dipole interactions. The band at 1659 cm^{-1} is found in a spectral area that most likely is related to loop structures. The lowest-frequency band appearing at 1610 cm^{-1} is probably related to amino acid side chains, possibly the amino acid tyrosine (*27*, *45*).

Figure 3a shows the score plot of the first and second principal component of the PCA of the second-derivative spectra of the amide I region from 1700 to 1600 cm^{-1}. The score plot reveals that the samples were clustering according to animal and salt concentration. PC 1 shows a clustering according to the animal (indicated with different colors), while PC 2 stretches out the variation according to the different salt concentrations (indicated with different symbols). The explained variances for PC 1 and PC 2 are 64 and 23%, respectively. PC 3 (not shown)

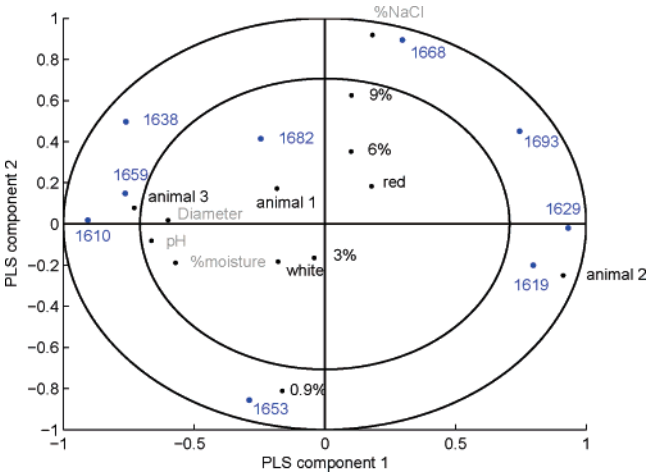

Figure 4. Correlation loading plot of ANOVA-PLSR with design (black) and chemical characteristics of the samples as *X* (weighted by 10^{-6}, gray) and selected variables of the negative second derivative of the amide I region of the FT-IR spectra as *Y* (blue). The explained variances of PLS components 1 and 2 were 17 and 15% for *X* and 47 and 25% for *Y*, respectively.

stretched out the variation due to the two different blocks, A and B, taken for every sampling condition. The explained variance for PC 3 is 8%. The samples of animal 2 possess the largest variation. **Figure 3b** presents the loadings of PC 1 and PC 2. The loading vector for the first PC reveals positive peaks for the variables between 1620 and 1635 cm^{-1} and the variables between 1690 and 1700 cm^{-1} and a negative tendency around 1638 and 1658 cm^{-1}. A positive peak between 1646 and 1659 cm^{-1} dominates the loading vector of PC 2, and it showed negative features around 1638 and 1666 cm^{-1}.

ANOVA-PLSR was used to investigate the effect of the design factors on the sample characteristics (**Table 1**) and FT-IR spectra. In the analysis, the **X**-matrix comprises the design parameters and sample characteristics (moisture, percent NaCl, diameter, and pH), while the **Y**-matrix consists of selected wavenumbers in the amide I range, which correspond to the bands shown in **Figure 2** (here, bands from the negative second-derivative spectrum). The sample characteristics were weighted by 10^{-6} to inhibit their influence on the regression between *X* and *Y*, while their correlation with the PLS components can be shown in the correlation loading plot. The resulting correlation loading plot shows both the correlation between the design and the measured data and the correlation between the design and the wavenumbers in the FT-IR spectra (**Figure 4**). The inner and outer circles in **Figure 4** refer to 50 and 100% explained variance, respectively. **Figure 4** shows that the meat qualities span the first PLS component with an explained variance of 17 and 47% for *X* and *Y*, respectively, while the salt concentrations span the second PLS component with an explained variance of 15 and 25% in *X* and *Y*, respectively. Animal 3 and the high pH of the sample have a positive correlation with the band related to the water content of the tissue (1638 cm^{-1}), with loop structures (1659 cm^{-1}), and with tyrosine content (1610 cm^{-1}). Those structures are also positively related to the large myofiber diameter and the high moisture content of the sample. Large amounts in aggregated β-sheet structures (1619, 1628, and 1693 cm^{-1}), on the other hand, are correlated with samples originating from animal 2 and low pH. No changes in α-helical structures (1653 cm^{-1}) appear to be related to differences between the animals. The results described above about correlations between design parameters, FT-IR band, and samples characteristics were confirmed by considering *p* values (not shown).

DISCUSSION

Ionic strength and pH are the main factors defining myofibrillar swelling and shrinkage and, thus, the water-holding capacity of meat. For cured meat, these are important factors affecting the salting process as well as the final meat quality. Even though the effect of salt and pH on the myofibrillar structure is well-known, very little is known about how the protein structure is affected and how this is related to the microstructural changes. In recent years, FT-IR microspectroscopy has been shown to be an excellent tool for the analysis of protein secondary structure in tissues. This is the first study that investigates protein secondary structural changes in pork due to salt by using FT-IR microspectroscopy. The results were compared to light microscopic structure observations.

To obtain meat with different pHs, the muscle samples were collected from animals with different preslaughter treatment. Two of the animals (1 and 2) had a pH_{24} of 5.6−5.7, while animal 3 had a pH_{24} of 6.5, being comparable to the pH of DFD (dark, firm, dry) meat, $pH_{24} > 6$ (*46*).

For all three animals, the pH decreased as the salt concentration increased. A similar observation was made by Thorarinsdottir et al. (*47*) during brine salting of cod. A higher pH was observed for the red part of the muscle than for the white part. This is in agreement with findings reported in the literature (*48*, *49*). Light microscopic images revealed differences in microstructural appearance between each animal. Animal 2 already had a widened extracellular space before salting, while animal 3 had the most compact structure. Whether these initial structural differences affect the salt uptake and/or salt-induced structural alterations is, to our knowledge, not known but should be investigated further.

It is well-known that salting leads to an increased swelling capacity of the muscle and increased spacing for water. Salt concentrations of >0.1 M (0.6%) in the muscle are thought to strengthen repulsive forces between filaments, and maximum swelling should be reached at ∼5−6% salt (*6*−*8*). In accordance with this fact, in our study, myofiber diameter and moisture content reached a maximum at NaCl concentrations of 3−6% in the muscle. Since we did not investigate the effects of additional brine concentrations between 3 and 6%, it was not possible to determine the exact NaCl concentration of the maximum moisture content and maximum myofiber diameter. For the salt concentrations that were used, samples of animal 3 reached maximum moisture and swelling at a lower salt concentration (3% brine) than samples from the other two animals (maximum at 6% brine). A possible reason may be the higher pH of animal 3, facilitating an increase in the net charge and thus increased swelling of the myofibers during salting (*8*, *50*). Irving et al. (*51*) observed a linear relationship between pH and transversal shrinkage of pork myofibrils in the pH region from 6.4 to 5.2, and Guignot et al. (*52*) reported almost constant myofilament spacing at pH >6. In addition to having a higher fiber diameter, higher moisture content, and higher pH, animal 3 was negatively correlated with aggregated β-sheet structures (1619, 1628, and 1693 cm^{-1}). Bertram et al. (*30*) reported after investigating heat-treated pork muscle that an increase in the levels of these β-structures leads to an increase in extramyofibrillar water content. This may imply that the animals with lower pH, especially animal 2 with an increased share of aggregated β-sheet structures, may also exhibit an increase in extramyofibrillar water content and a related higher drip loss. This is in accordance with the lower moisture content of these samples compared to those with higher pHs. Furthermore, Bertram et al. (*30*) considered the band at 1639 cm^{-1}, which, in this study, is highly related to high pH and animal 3, to be a potential indicator for tightly bound water. In our study, we found the high moisture content of the high-pH animal also to be related to this band, while the two other animals and less moisture were inversely correlated with this band.

As shown in the correlation loading plot, larger amounts of α-helical structures (1653 cm^{-1}) were characteristic of samples with low salt content. At the same time, high-salt content samples are related to a higher level of nonhydrogenated C═O groups (1668 cm^{-1}). Stafford (*53*) investigated the effect of neutral salts on the stability of the α-helical coiled coil of rabbit skeletal myosin by using circular dichroism and optical rotation measurements. He reported that Cl^- ions had a tendency to destabilize the structure of the myosin coiled coil in or near the S-2/LMM junction. They stated that a higher level of nonhydrogenated C═O groups (1668 cm^{-1}) may be caused by similar structural alterations. This supports our findings that the share of α-helical structures (1653 cm^{-1}) is higher in samples with low salt content and that the level of nonhydrogenated C═O groups (1668 cm^{-1}) is increased at higher salt concnetrations. The observed salt-induced structural changes in our experiment also are supported by the findings of Offer et al. (*8*). They suggested not only that salt-induced swelling was explained by an increase in the strength of electrostatic repulsive forces but also that the main action of NaCl was to depolymerize the thick filaments and that the mechanism for swelling was entropic.

The red and white muscles did not exhibit any significant differences in the amide I region of the IR spectra. If effects are present, they are minor compared to the differences introduced by salting and differences in raw material.

Overall, this study using FT-IR microscopy in combination with light microscopy demonstrated that changes observed in microstructure, i.e., myofiber diameter and change in shape, are a function of salting. In addition, the study indicated that moisture content is related to changes in protein secondary structure. Effects of salting and animal differences, however, appeared not to affect the same secondary structure motifs. With an increase in salt concentration in the muscle, the level of α-helical components of myofibrillar proteins decreased and the level of nonhydrogenated C═O groups increased. In contrast, the level of aggregated β-strands was increased for animal 2 while it was least for animal 3 (high pH). This may also explain the more amorphous appearance in the micrographs, particularly at the higher NaCl concentrations of animal 3 compared to animals 1 and 2.

It is likely that the three major proteins of the myofibers (myosin, actin, and titin make up 84%) are the main contributors to the FT-IR signal in the amide I region, but it is not possible to differentiate precisely the molecules or region of the molecules in which changes occur that cause changes in the FT-IR spectra. Changes related to α-helical structures may possibly be due to changes in the myosin rod, while changes in β-structures may be caused by changes in the myosin head, since myosin makes up more than 50% of the myofibrillar proteins. However, contributions from other proteins cannot be ruled out.

In the future, it may be useful to investigate the myofibrillar proteins and their changes caused by NaCl separately, to gain deeper insight into the changes found in the FT-IR spectra, though one must be aware of the fact that this will have to happen in a matrix different from the one presented by natural muscle tissue, which may therefore cause changes in the spectral signatures.

ACKNOWLEDGMENT

We thank Marianne Rasmussen, Grethe Enersen, and Karin Solgaard for their technical assistance.

LITERATURE CITED

(1) Arnau, J.; Guerrero, L.; Sarraga, C. The effect of green ham pH and NaCl concentration on cathepsin activities and the sensory characteristics of dry-cured hams. *J. Sci. Food Agric.* **1998**, *77*, 387−392.

(2) Guerrero, L.; Gou, P.; Arnau, J. The influence of meat pH on mechanical and sensory textural properties of dry-cured ham. *Meat Sci.* **1999**, *52*, 267−273.

(3) Ruiz-Ramirez, J.; Arnau, J.; Serra, X.; Gou, P. Relationship between water content, NaCl content, pH and texture parameters in dry-cured muscles. *Meat Sci.* **2005**, *70*, 579−587.

(4) Garcia-Rey, R. M.; Garcia-Garrido, J. A.; Quiles-Zafra, R.; Tapiador, J.; Luque de Castro, M. D. Relationship between pH before salting and dry-cured ham quality. *Meat Sci.* **2004**, *67*, 625−632.

(5) Hamm, R. Biochemistry of meat hydration. In *Advances in Food Research*; Chichester, C. O., Mark, E. M., Eds.; Academic Press: New York, 1960; pp 355−463.

(6) Honikel, K. O. The meat aspects of water and food quality. In *Water and food quality*; Hardman, T. M., Ed.; Elsevier Applied Science: London, 1989.

(7) Offer, G.; Trinick, J. On the mechanism of water holding in meat: The swelling and shrinking of myofibrils. *Meat Sci.* **1983**, *8*, 245−281.

(8) Offer, G.; Knight, P. In *Developments in meat science*; Lawrie, R., Ed.; Elsevier Science Publishers Ltd.: Barking, Essex, U.K., 1988.

(9) Wilding, P.; Hedges, N.; Lillford, P. J. Salt-induced swelling of meat: The effect of storage time, pH, ion-type and concentration. *Meat Sci.* **1986**, *18*, 55−75.

(10) Fretheim, K.; Samejima, K.; Egelandsdal, B. Myosins from red and white bovine muscles: Part 1. Gel strength (elastisticity) and water-holding capacity of heat-induced gels. *Food Chem.* **1986**, *22*, 107−121.

(11) Offer, G.; Knight, P.; Jeacocke, R.; Almond, R.; Cousins, T.; Elsey, J.; Parsons, N.; Sharp, A.; Starr, R.; Purslow, P. The structural basis of the water-holding, appearance and toughness of meat and meat-products. *Food Microstruct.* **1989**, *8*, 151−170.

(12) Knight, P.; Elsey, J.; Hedges, N. The role of the endomysium in the salt-induced swelling of muscle fibres. *Meat Sci.* **1989**, *26*, 209−232.

(13) Meyer, C.; Egelandsdal, B. Low deformation and water holding measurements of whole and comminuted meat originating from 2 muscles of different fibre type composition. *J. Texture Stud.* **1992**, *23*, 25−45.

(14) Egelandsdal, B.; Martinsen, B. K.; Autio, K. Rheological parameters as predictors of protein functionality: A model study using myofibrils from red and white bovine muscles. *Meat Sci.* **1995**, *39*, 97−111.

(15) Craig, R. W.; Padron, R. In *Myology*, 3rd ed.; Engel, A. G., Franzini-Armstrong, C., Eds.; McGraw-Hill: New York, 2004.

(16) Kabsch, W.; Vandekerckhove, J. Structure and function of actin. *Annu. Rev. Biophys. Biomol. Struct.* **1992**, *21*, 49−76.

(17) Uchida, K.; Harada, I.; Nakauchi, Y.; Maruyama, K. Structural-properties of connectin studied by ultraviolet resonance Raman-spectroscopy and infrared dichroism. *FEBS Lett.* **1991**, *295*, 35−38.

(18) Kimura, S.; Matsuura, T.; Ohtsuka, S.; Nakauchi, Y.; Matsuno, A.; Maruyama, K. Characterization and localization of α-connectin (Titin-1): An elastic protein isolated from rabbit skeletal muscle. *J. Muscle Res. Cell Motil.* **1992**, *13*, 39−47.

(19) Politou, A. S.; Gautel, M.; Pfuhl, M.; Labeit, S.; Pastore, A. Immunoglobulin-type domains of titin: Same fold, different stability. *Biochemistry* **1994**, *33*, 4730−4737.

(20) Muhle-Goll, C.; Nilges, M.; Pastore, A. H-1 and N-15 NMR resonance assignments and secondary structure of titin type I domains. *J. Biomol. NMR* **1997**, *9*, 2−10.

(21) Trinick, J.; Tskhovrebova, L. Titin: A molecular control freak. *Trends Cell Biol.* **1999**, *9*, 377−380.

(22) Wright, D. J.; Wilding, P. Differential scanning calorimetric study of muscle and its proteins: Myosin and its subfragments. *J. Sci. Food Agric.* **1984**, *35*, 357−372.

(23) Barbut, S.; Findlay, C. J. Influence of sodium, potassium and magnesium-chloride on thermal-properties of beef muscle. *J. Food Sci.* **1991**, *56*, 180−182.

(24) Fiala, M.; Honikel, K. O. The application of the differential scanning calorimetry. *Fleischwirtschaft* **1995**, *75*, 1013−1018.

(25) Diem, M.; Boydston-White, S.; Chiriboga, L. Infrared spectroscopy of cells and tissues: Shining light onto a novel subject. *Appl. Spectrosc.* **1999**, *53*, 148A−161A.

(26) Diem, M.; Romeo, M.; Boydston-White, S.; Miljkovic, M.; Matthäus, C. A decade of vibrational micro-spectroscopy of human cells and tissue. *Analyst* **2004**, *129*, 880−885.

(27) Fabian, H.; Mäntele, W. Infrared spectroscopy of proteins. In *Handbook of Vibrational Spectroscopy*; Chalmers, J. M., Griffiths, P. R., Eds.; John Wiley & Sons Ltd.: Chichester, U.K., 2002; pp 3499−3425.

(28) Barth, A.; Zscherp, C. What vibrations tell us about proteins. *Q. Rev. Biophys.* **2002**, *35*, 369−430.

(29) Kirschner, C.; Ofstad, R.; Skarpeid, H.-J.; Høst, V.; Kohler, A. Monitoring of denaturation processes in meat by FT-IR microspectroscopy. *J. Agric. Food Chem.* **2004**, *52*, 3920−3929.

(30) Bertram, H. C.; Kohler, A.; Ofstad, R.; Böcker, U.; Andersen, H. J. Heat-induced changes in myofibrillar protein structures and myowater of two pork qualities. A combined FT-IR spectroscopy and low-field NMR relaxometry study. *J. Agric. Food Chem.* **2006**, *54*, 1740−1746.

(31) Bertram, H. C.; Schäfer, A.; Rosenvold, K.; Andersen, H. J. Physical changes of significance for early post mortem water distribution in porcine *M. longissimus*. *Meat Sci.* **2004**, *66*, 915−924.

(32) Henckel, P.; Karlsson, A.; Oksbjerg, N.; Petersen, J. S. Control of post mortem pH decrease in pig muscles: Experimental design and testing of animal models. *Meat Sci.* **2000**, *55*, 131−138.

(33) Karlsson, A. H.; Rosenvold, K. The calibration temperature of pH-glass electrodes: Significance for meat quality classification. *Meat Sci.* **2002**, *62*, 497−501.

(34) Lillie, R. D.; Fullmer, H. M. *Histopathologic technic and practical histochemistry*; McGraw-Hill: New York, 1976.

(35) Engdahl, A.; Kolar, K. Metodeforskrift 22.6.93 Koksaltbestämning med Corning 926 Chloride Analyzer, Köttforskningsinstitut i Kävlinge, 1993.

(36) Nordisk Metodikkommite for næringsmidler, NMKL-metode nr 23, 1991.

(37) Martens, H.; Stark, E. Extended multiplicative signal correction and spectral interference subtraction: New preprocessing methods for near-infrared spectroscopy. *J. Pharm. Biomed. Anal.* **1991**, *9*, 625−635.

(38) Kohler, A.; Kirschner, C.; Oust, A.; Martens, H. Extended multiplicative signal correction as a tool for separation and characterization of physical and chemical information in Fourier transform infrared microscopy images of cryo-sections of beef loin. *Appl. Spectrosc.* **2005**, *59*, 707−716.

(39) DeNoyer, L. K.; Dodd, J. G. Smoothing and derivatives in spectroscopy. In *Handbook of Vibrational Spectroscopy*; Chalmers, J. M., Griffiths, P. R., Eds.; John Wiley & Sons Ltd.: Chichester, U.K., 2002; pp 2173−2183.

(40) Martens, H.; Martens, M. *Multivariate Analysis of Quality: An Introduction*; John Wiley & Sons, Ltd.: Chichester, U.K., 2001.

(41) Wold, S.; Martens, H.; Wold, H. The multivariate calibration problem in chemistry solved by the PLS method. In *Proceedings of the Conference on Matrix Pencils*; Springer-Verlag, Heidelberg, Germany, 1983; pp 286−293.

(42) Jackson, M.; Mantsch, H. H. The use and misuse of FTIR spectroscopy in the determination of protein-structure. *Crit. Rev. Biochem. Mol. Biol.* **1995**, *30*, 95−120.
(43) Jackson, M.; Choo, L. P.; Watson, P. H.; Halliday, W. C.; Mantsch, H. H. Beware of connective-tissue proteins: Assignment and implications of collagen absorptions in infrared-spectra of human tissues. *Biochim. Biophys. Acta* **1995**, *1270*, 1−6.
(44) Sokrates, G. *Infrared and Raman Characteristic Group Frequencies. Tables and Charts*, 3rd ed.; John Wiley & Sons Ltd.: Chichester, U.K., 2001.
(45) Chu, H. L.; Liu, T. Y.; Lin, S. Y. Effect of cyanide concentrations on the secondary structures of protein in the crude homogenates of the fish gill tissue. *Aquat. Toxicol.* **2001**, *55*, 171−176.
(46) Greaser, M. L. Conversion of muscle to meat. In *Muscle as food*; Bechtel, P. J., Ed.; Academic Press: London, 1986; pp 37−102.
(47) Thorarinsdottir, K. A.; Arason, S.; Bogason, S. G.; Kristbergsson, K. The effects of various salt concentrations during brine curing of cod (Gadus morhua). *Int. J. Food Sci. Technol.* **2004**, *39*, 79−89.
(48) Lawrie, R. A. *Lawrie's Meat Science*, 6th ed.; Woodhead Publishing Ltd.: Cambridge, U.K., 1998.
(49) Rao, M. V.; Gault, N. F. S. The influence of fibre-type composition and associated biochemical characteristics on the acid buffering capacities of several beef muscles. *Meat Sci.* **1989**, *26*, 5−18.
(50) Ofstad, R.; Kidman, S.; Myklebust, R.; Olsen, R. L.; Hermansson, A. M. Liquid-holding capacity and structural-changes in comminuted salmon (Salmo-Salar) muscle as influenced by pH, salt and temperature. *Food Sci. Technol.* **1995**, *28*, 329−339.
(51) Irving, T. C.; Swatland, H. J.; Millman, B. M. Effect of pH on myofilament spacing in pork measured by X-ray-diffraction. *Can. Inst. Food Sci. Technol. J.* **1990**, *23*, 79−81.
(52) Guignot, F.; Vignon, X.; Monin, G. Postmortem evolution of myofilament spacing and extracellular-space in veal muscle. *Meat Sci.* **1993**, *33*, 333−347.
(53) Stafford, W. F. Effect of various anions on the stability of the coiled coil of skeletal-muscle myosin. *Biochemistry* **1985**, *24*, 3314−3321.

Received for review January 20, 2006. Revised manuscript received June 15, 2006. Accepted June 29, 2006. This work was supported by Grant 153381/140 financed by the Research Council of Norway.

JF060178Q